Review

Ground-Glass Opacity at CT: The ABCs

Jannette Collins[1] and Eric J. Stern[2]

Ground-glass opacity (GGO) describes a finding on high-resolution CT (HRCT) of the lungs in which is seen "hazy increased attenuation of lung, with preservation of bronchial and vascular margins; caused by partial filling of air spaces, interstitial thickening, partial collapse of alveoli, normal expiration, or increased capillary blood volume....Not to be confused with 'consolidation,' in which bronchovascular margins are obscured. May be associated with an air bronchogram" [1]. This finding is often occult on chest radiographs. In 1989, Klein and Gamsu [2] described "hazy increased density" as a pattern of diffuse lung disease, referring to the "fine granular appearance" that has been termed GGO. Although GGO is a nonspecific finding, in certain clinical circumstances it can suggest a specific diagnosis, indicate a potentially treatable disease, or guide a bronchoscopist or surgeon to an appropriate area for biopsy. In 1993, the significance of GGO was described by Remy-Jardin et al. [3], and in the same year Engeler et al. [4] published a pictorial essay of this entity. The interest in GGO is further illustrated by a section in an HRCT textbook [5] and six articles [6–11]. The differential diagnosis for GGO is lengthy, which can make interpretation of HRCT frustrating. Because GGO is a frequent finding on HRCT, a simplistic approach to the differential diagnosis, the ABCs, is offered in this review.

GGO can be patchy, resulting in a mosaic pattern of lung attenuation. This mosaic pattern is seen in infiltrative lung diseases, airway abnormalities, and primary vascular disease [12]. The distinction between these three entities can be made by observing the size of the pulmonary vessels in the area of increased lung attenuation (increased in both airway disease and vascular disease, but not in infiltrative disease) and air trapping on expiratory scans (indicating airway disease). This review is limited to a discussion of infiltrative processes.

Pitfalls in the Interpretation of GGO on HRCT

Recognition of GGO is based on a subjective assessment of lung attenuation. Although attenuation of the lung is closely related to density, which suggests that CT should provide an objective quantifictation of GGO, many parameters interfere with lung density and make attenuation measurements unreliable. These parameters were previously discussed by Remy-Jardin et al. [3] and, more recently, by Primack et al. [13]. Narrow window width and level can erroneously create the appearance of GGO by magnifying small structures. A recommended range for window width and level is 1500–2000 H and −500 to −700 H, respectively [3]. Choosing the correct current is also important. A tube current that is too low will produce excessive noise, which can mimic GGO. Generally, a current of 240–400 mA is acceptable [5]. In our experience, a current of 250–350 mA is adequate for most patients, with larger patients requiring increased current. Zwirewich et al. [14] evaluated both low-exposure (20 mA) and conventional exposure (200 mA) HRCT, both with a 2-sec scan time, and found that the low-exposure technique failed to show GGO in two of 10 cases in which GGO was evident on the high-exposure scans. A kilovoltage of 120–140 and a matrix of 512 × 512 are recommended [5]. Although filming six images on one 14 × 17 inch (36 × 43 cm) sheet of film has been recommended [5], we prefer to film the images 12-on-one, which uses fewer pages of film. Further improvement in the image quality can be obtained by decreasing the field of view and targeting the image to one lung [15, 16]. Collimation should be 1.0–1.5 mm because GGO may not be visualized with thicker collimation caused by volume averaging. Furthermore, thicker collimation may result in pseudo-GGO, which, when resolved with thin-collimation HRCT, can be recognized as linear atelectasis or other obvious disease. For this reason, GGO should be confirmed on HRCT. A high-spatial-frequency algorithm should be used, and the scan time should be as short as possible, generally 1–2 sec.

The lung attenuation normally increases with expiration. This increased attenuation can mask underlying GGO from infiltrative lung disease or create an appearance of diffuse lung disease if the expiratory nature of the examina-

Received October 31, 1996; accepted after revision February 24, 1997.

Presented at the annual meeting of the American Roentgen Ray Society, Boston, May 1997.

[1]Department of Radiology, University of Wisconsin Hospital & Clinics, E3/311 CSC, 600 Highland Ave., Madison, WI 53792-3252. Address correspondence to J. Collins.

[2]Department of Radiology, Harborview Medical Center, Box 359728, University of Washington, Seattle, WA 98104.

AJR 1997;169:355–367 0361–803X/97/1692–355 © American Roentgen Ray Society

tion is not appreciated. The tracheal configuration changes from round in inspiration to flat or crescent-shaped in expiration and can be used to determine whether the CT scan was performed in inspiration or expiration.

Subpleural opacities caused by microatelectasis are frequently identified in the dependent portions of the lungs. These dependent opacities generally consist of reticular, linear, and ground-glass opacities and can be confused with or mask true infiltrative lung disease. When it is clinically important to make the distinction between infiltrative lung disease and non–disease-dependent opacities, repeated imaging with the patient in the prone position is recommended. This procedure will result in dependent opacities shifting to the anterior subpleural areas and true infiltrative lung disease persisting in the nondependent posterior lungs.

Cardiac and respiratory motion can create pseudo-GGO, which can be distinguished from true GGO by recognizing blurring and double images of vessels and fissures.

ABCs of GGO

A differential diagnosis for GGO is offered that includes disorders that begin with the letters A–G (Table 1). The disorders listed in this review were chosen because they have been included in the differential diagnosis of GGO by others in the literature and because they commonly result in GGO as the sole manifestation of the parenchymal process or as a dominant finding on HRCT. Because GGO can represent either interstitial or alveolar processes, beyond the resolution of the HRCT technique the complete differential diagnosis is long (Fig. 1).

A

Alveolar proteinosis.—Pulmonary alveolar proteinosis is a disease of the lung that results in filling in of the alveoli by a periodic acid–Schiff–positive proteinaceous material rich in lipid [17, 18]. The underlying cause is speculated to be dust (particularly silica) exposure or an immunologic disturbance (caused by AIDS or other immunodeficiency, hematologic and lymphatic malignancy, or chemotherapy). Superinfections occur, most notably with nocardiosis [19]. In 1988, Godwin et al. [19] described the CT features of nine patients with pulmonary alveolar proteinosis. All patients had air-space opacity on CT (not differentiated as to GGO or consolidation), and the authors reported that an interstitial pattern was frequent and sometimes predominated. Murch and Carr [20] described a characteristic CT appearance in six patients with pulmonary alveolar proteinosis. The pattern seen in all patients was of opacified lung with a "diffuse uniform grey appearance" (ground-glass), with an overlying branching pattern of white linear structures forming geometric shapes and outlining polygonal, triangular, and square forms. This pattern was referred to as "crazy paving" (Fig. 2). Histologically, the ground-glass component represents partial filling of alveoli with proteinaceous material and edematous, thickened interlobular septa.

Acute chest syndrome of sickle cell disease.—Acute chest syndrome of sickle cell disease refers to the clinical syndrome of chest pain, fever, prostration, and pulmonary opacities on chest radiographs. The opacities seen on chest radiographs and chest CT scans represent pneumonia or infarction due to microvascular occlusion, and clinical and radiographic differentiation between the two causes is usually not possible [21, 22]. Bhalla et al. [23] studied the CT scans of 10 patients with acute chest syndrome and found absence or paucity of arterioles and venules and areas of GGO in nine patients. The areas of GGO were geographic, patchy, and multifocal in some cases and confluent with total lobar involvement in others and were attributed to early hemorrhagic edema caused by sudden occlusion of pulmonary artery flow.

TABLE 1 ABCs of Ground-Glass Opacity

ABCs	Causes
A	Alveolar proteinosis
	Acute chest syndrome
	Acute lung transplant rejection
	Acute respiratory distress syndrome
B	Blood
	Bronchiolitis obliterans organizing pneumonia
	Bronchoalveolar lavage
	Bronchiolitis-associated interstitial lung disease
C	Cytomegalovirus and other pneumonias (*Pneumocystis carinii*)
	Cancer and lymphoproliferative disorders
	Collagen vascular disease
	Contusion
D	Drug toxicity
	Desquamative interstitial pneumonitis
E	Extrinsic allergic alveolitis
	Eosinophilic pneumonia
	Edema
F	Fibrosis
G	Granulomatous disease (e.g., sarcoidosis)

Acute lung transplant rejection.—New lung opacities in the immediate period after lung transplantation can be due to infection, rejection, reperfusion edema, or fluid overload. Reperfusion edema is manifested by perihilar interstitial and alveolar opacities on the first postoperative chest radiograph. This process can worsen over several days but generally stabilizes or resolves within 2 weeks. During this period, the differentiation between reperfusion edema, infection, and rejection is difficult both clinically and radiographically. Any new opacities after the immediate postoperative period are suspicious for rejection or infection (Fig. 3). After reviewing 190 transbronchial biopsies and concurrent HRCT scans in 32 lung transplant patients, Loubeyre et al. [24] documented a 21% incidence of acute rejection histologically, with HRCT being 65% sensitive and 85% specific for this diagnosis. The study included patients evaluated with bronchoscopy and CT from 2 weeks to 2 years after transplantation. The only significant HRCT finding in acute rejection was GGO, seen in 65% of patients with rejection, which was patchy and localized in mild rejection and widespread in severe rejection. GGO was always present in the most severe grades of acute rejection. The GGO seen in acute rejection represents an alveolitislike process. On histologic samples of acute rejection, extension of the inflammatory cell infiltrate into perivascular and peribronchioloalveolar septa and air spaces occurs, especially when the grade of rejection is high. The main differential diagnosis in this group of patients is cytomegalovirus (CMV) pneumonia, which can have an identical radiographic appearance.

Adult respiratory distress syndrome.—Adult respiratory distress syndrome (ARDS) is characterized by refractory hypoxemia and respiratory distress caused by nonhydrostatic pulmonary edema (Fig. 4). Leaky capillary membranes lead to extravasation of protein-rich fluid into the interstitial and alveolar spaces of the lung, leading to a decrease in normally inflated lung volume and a decrease in lung compliance. Numerous precipitating factors are known, including aspiration, contusion, smoke inhalation, and sepsis. Patients surviving ARDS can have little pulmonary sequelae but may develop severe lung fibrosis. The true rate of conversion of ARDS to interstitial fibrosis is unknown because follow-up lung biopsy is so rarely performed [25]. CT is seldom used to examine patients with ARDS because of the difficulty in transporting critically ill patients to the radiology

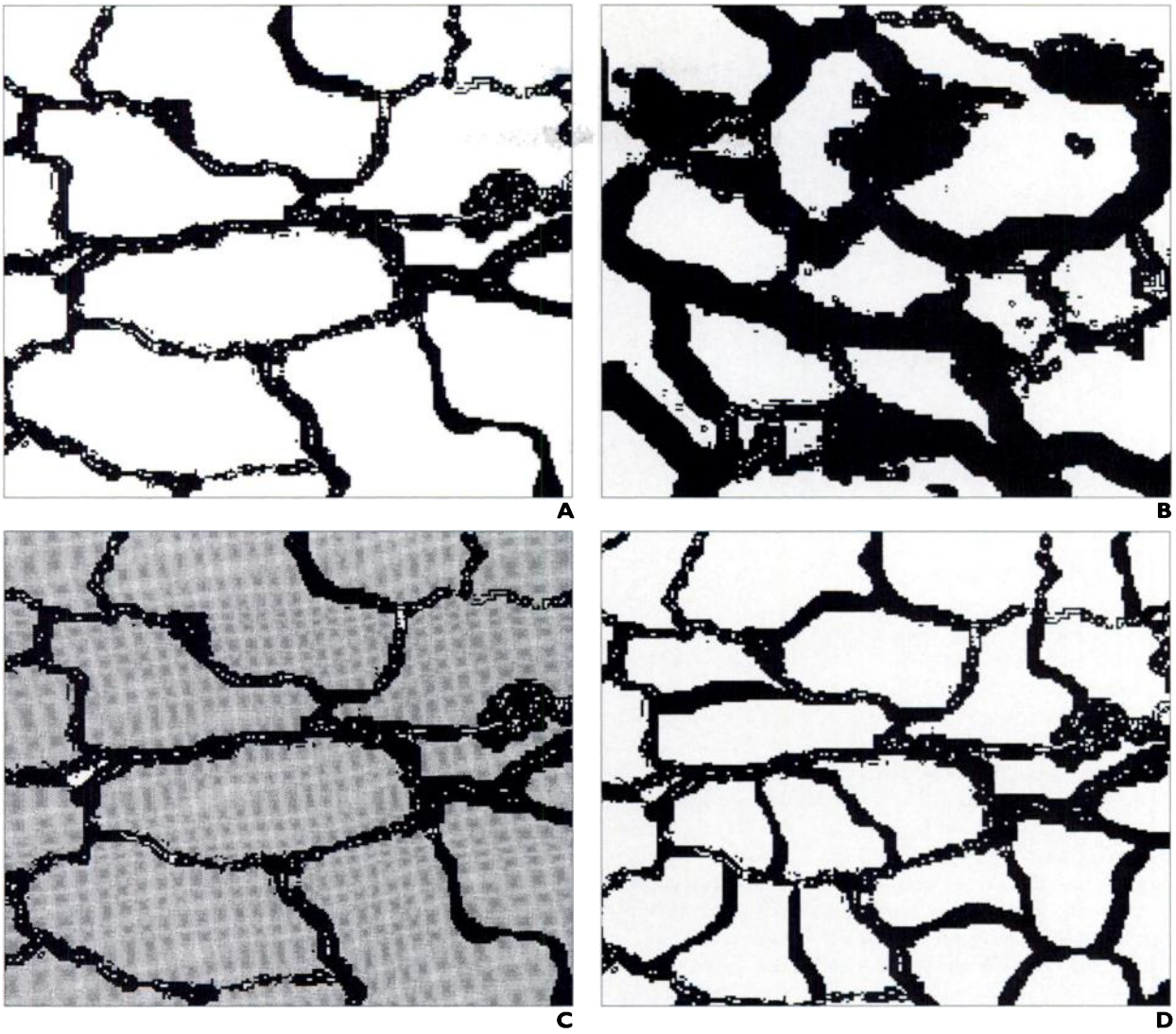

Fig. 1.—Diagrammatic representations of different causes of ground-glass opacity (GGO) on CT chest scans. Each box represents a pixel on a CT scan. Diagrams highlight nonspecific nature of GGO.

A, Pixel contains normal lung parenchyma at full inspiration with normal alveolar walls and alveolar air spaces. Normal amounts of air, blood, and tissue in pixel will yield a certain expected Hounsfield attenuation and will be assigned gray-scale value (e.g., –800 H).

B, Pixel shows thickening of interstitium of lung, which may result from either inflammatory or fibrotic response to insult (e.g., alveolitis or microfibrosis), which in turn creates more "tissue" per pixel relative to air, thus increasing the Hounsfield value assigned that pixel (e.g., –650 H).

C, Pixel shows fluid filling alveoli (e.g., edema), again increasing Hounsfield value assigned that pixel.

D, Pixel shows normal parenchyma at end of exhalation. Note increased number of alveolar walls per pixel and less air than in **A**. Results include increased gray-scale values.

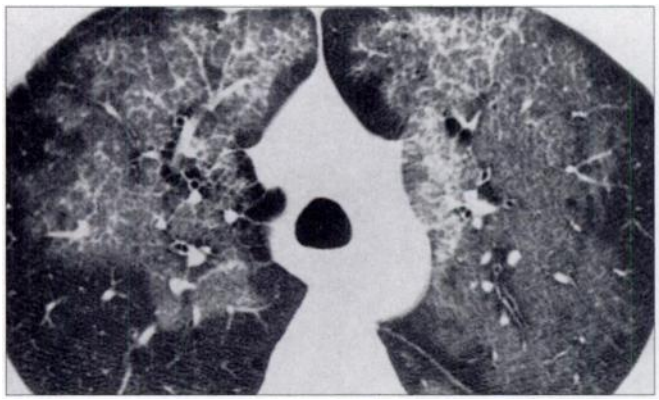

Fig. 2.—37-year-old man with pulmonary alveolar proteinosis. High-resolution CT scan shows ground-glass opacity of alveolar spaces and thickening of interlobular septa with no architectural distortion. Note typical polygonal shapes called "crazy-paving." Also note sharp demarcation from surrounding normal lung tissue, creating geographic pattern.

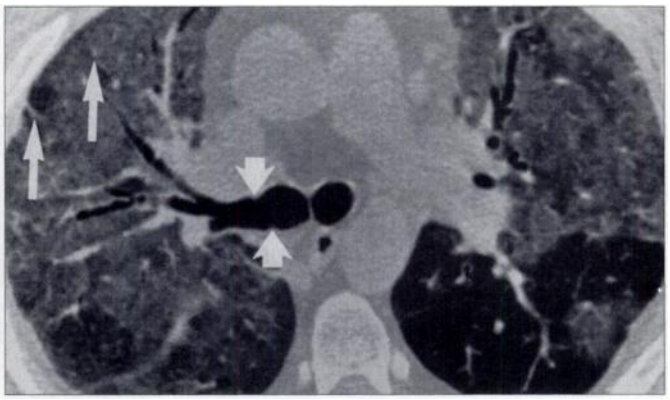

Fig. 3.—38-year-old man 23 days after bilateral lung transplantation for idiopathic pulmonary fibrosis with acute lung transplant rejection. High-resolution CT scan shows bilateral patchy ground-glass opacity and interlobular septal thickening (*long arrows*). Right bronchial anastomosis is normal, without stricture or dehiscence, and small indentations anteriorly and posteriorly result from telescoping technique of surgical anastomosis (*short arrows*). Transbronchial biopsy revealed bronchiolitis obliterans organizing pneumonia, mild rejection, and no active infection.

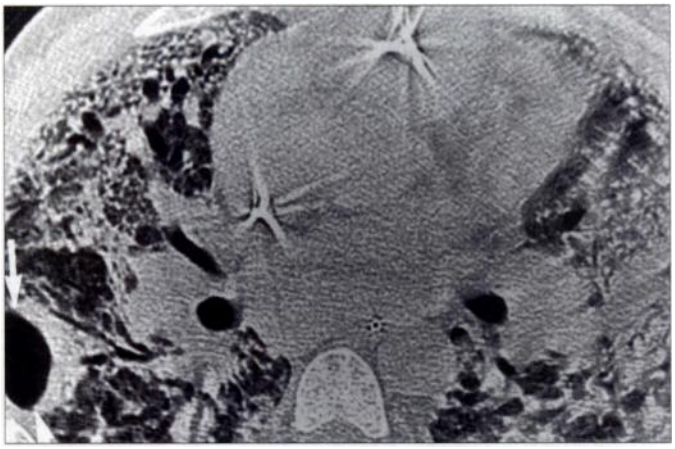

Fig. 4.—37-year-old man after recent resection of intracranial neoplasm who developed acute respiratory failure and adult respiratory distress syndrome requiring prolonged intubation. High-resolution CT scan shows bilateral diffuse mixed consolidation and ground-glass opacity, pneumatocele (*arrows*) and small cystic spaces caused by barotrauma, and bronchiolar dilatation.

department. Tagliabue et al. [26] reviewed the CT scans of 74 patients with ARDS and observed lung opacities that were bilateral and dependent in most of the patients (92% and 86%, respectively). These researchers reported only an 8% incidence of GGO. Likewise, Owens et al. [27] studied the serial changes in the appearances of the lungs on CT scans in eight patients with ARDS. Early in the course, all patients had GGO on CT, which persisted on follow-up CT in 50% of patients. Other findings included parenchymal distortion, multifocal areas of consolidation, and reticular and linear opacities. On follow-up scans, clearing of consolidation occurred in all patients, but GGO persisted in four of eight patients. This persistent GGO probably represented interstitial thickening (by edema, inflammatory cells, or fibrosis), partial filling of the air spaces, or a combination of the two.

B

Blood.—Pulmonary hemorrhage can be diffuse, patchy, or focal, depending on the underlying cause. Pulmonary–renal syndromes that cause pulmonary hemorrhage include Goodpasture's syndrome, Wegener's granulomatosis, systemic lupus erythematosus, Henoch-Schönlein purpura, mixed connective-tissue disease, and other vasculitides. Some of these processes also occur without renal disease. Other causes of pulmonary hemorrhage include anticoagulant use, disseminated intravascular coagulation, thrombocytopenia, leukemia, acute lung injury (ARDS, toxic inhalation, oxygen toxicity), aspiration of blood, drug toxicity, blunt or penetrating trauma, and mitral stenosis [28]. In the acute phase, HRCT scans show consolidation or GGO (Fig. 5). In the subacute phase, CT scans will show 1- to 3-mm nodules distributed in a uniform fashion common with GGO and interlobular septal thickening [29]. Pulmonary hemorrhage can occur as a halo of GGO around a focal area of lung consolidation (Figs. 6 and 7). This ground-glass halo was reported by Kuhlman et al. [30] to be a clue to the diagnosis of early invasive pulmonary aspergillosis in leukemic patients. Those authors speculated that the pathologically identified peripheral ring of hemorrhage or hemorrhagic infarction surrounding target lesions corresponds to the CT halo zone of GGO surrounding invasive pulmonary aspergillosis lesions on CT scans. Primack et al. [31] reported several infectious and noninfectious causes of the CT halo sign, including metastases and Kaposi's sarcoma. The study of these researchers showed that in most patients hemorrhagic nodules can be distinguished from nonhemorrhagic nodules by the presence of a halo of GGO (Figs. 8 and 9). Another more recently described cause of focal GGO, or nodule with a surrounding ground-glass halo representing hemorrhage, is the pseudonodule resulting from transbronchial lung biopsy (Fig. 10). This pseudonodule was described by Kazerooni et al. [32], who reviewed 141 CT scans in 40 patients who had undergone lung transplantation and transbronchial biopsies. These researchers found nodules representing biopsy-related injury in 30% of the studied patients and concluded that when these nodules are detected within a few weeks of transbronchial biopsy, biopsy-related lung injury in addition to pulmonary infection and allograft rejection should be considered.

Bronchiolitis obliterans organizing pneumonia.—Bronchiolitis obliterans is a disease characterized histologically by the presence of granulation tissue plugs that occupy and often

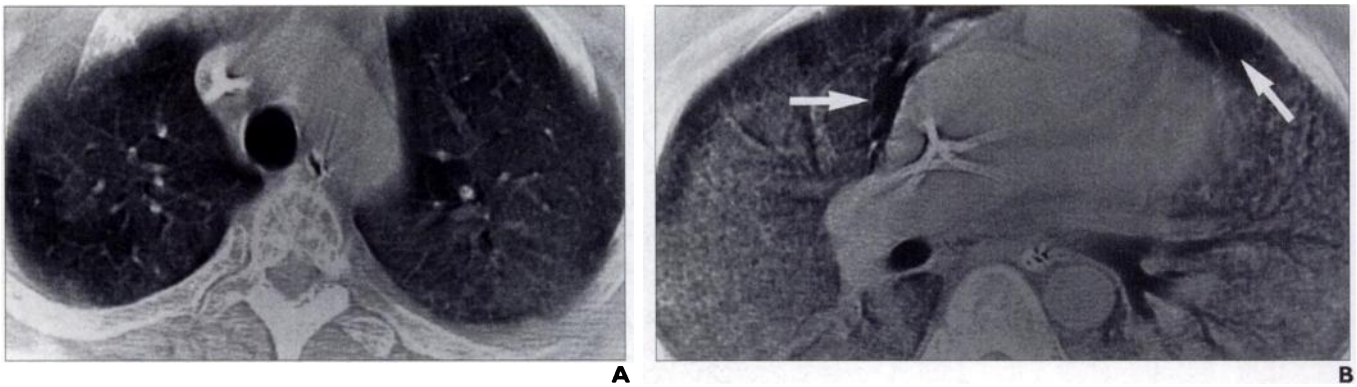

Fig. 5.—25-year-old man with diffuse alveolar hemorrhage who underwent ablative chemotherapy, total body irradiation, and allogeneic bone marrow transplantation for multiple myeloma and then developed acute respiratory failure requiring mechanical ventilation and eventual tracheostomy.
A, CT scan obtained 25 days after transplantation shows bilateral patchy ground-glass opacity (GGO) correlating with bronchoalveolar lavage findings of blood only (no evidence of infection).
B, CT scan obtained 18 days after **A** shows increased bilateral GGO, small cystic areas bilaterally (representing pulmonary interstitial emphysema), and pneumomediastinum (*arrows*) due to barotrauma, all of which correlate with clinical diagnosis of adult respiratory distress syndrome.

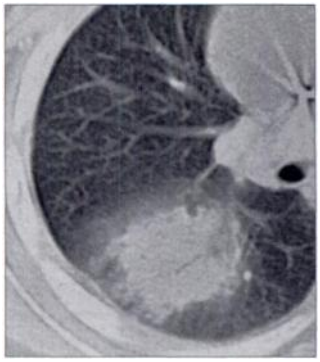

Fig. 6.—8-year-old boy with invasive pulmonary aspergillosis who was treated with chemotherapy for acute myelogenous leukemia. CT scan shows consolidation of right lower lobe, with halo of ground-glass opacity. Biopsy of mass confirmed diagnosis of invasive aspergillosis.

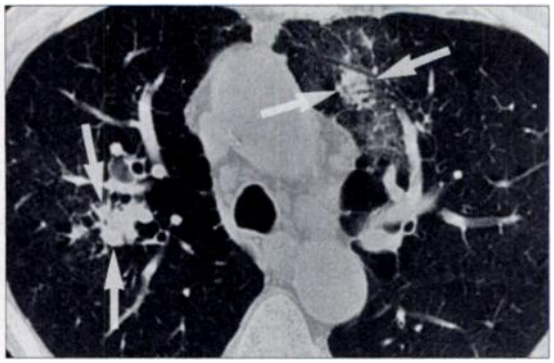

Fig. 7.—62-year-old man with invasive pulmonary aspergillosis 3 months after orthotopic heart transplantation. High-resolution CT scan shows bilateral upper lobe masses with ground-glass halos (*arrows*), correlating with histologic diagnosis of invasive aspergillosis.

occlude respiratory bronchioles and alveolar ducts (Fig. 11). In pure bronchiolitis obliterans, the surrounding lung parenchyma is normal. When bronchiolitis obliterans is accompanied by organizing pneumonia extending into the surrounding centriacinar alveoli, the term bronchiolitis obliterans organizing pneumonia (BOOP) is applied [33]. Although bronchiolitis results from a specific cause in many cases (exposure to fumes and toxic gases, infection, connective-tissue diseases, organ transplantation), BOOP (also referred to as cryptogenic organizing pneumonia) is commonly idiopathic (Fig. 12). Clinically, BOOP usually presents as a subacute illness with signs and symptoms including cough, dyspnea, fever, sputum expectoration, malaise, and weight loss [34]. BOOP may resolve spontaneously. With steroid treatment, clinical and radiographic signs clear in

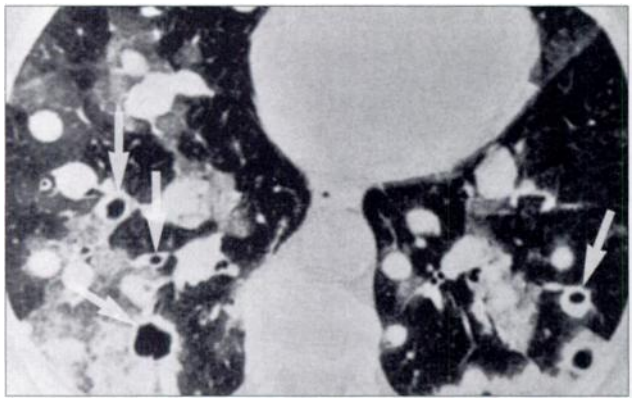

Fig. 8.—63-year-old-woman with metastatic melanoma involving multiple organ systems. High-resolution CT scan shows multiple well-circumscribed nodules with surrounding halos of ground-glass opacity representing hemorrhage. Many nodules are cavitary, an unusual finding in malignant melanoma (*arrows*).

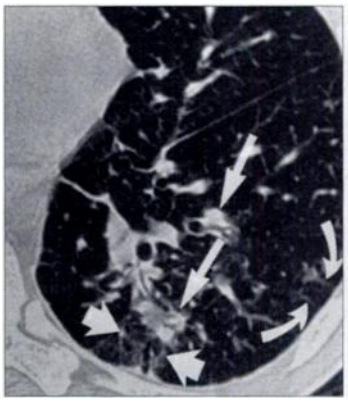

Fig. 9.—34-year-old man with AIDS and Kaposi's sarcoma. High-resolution CT scan shows irregular opacities in bronchovascular distribution (*long arrows*) with surrounding ground-glass opacity (GGO) (*short arrows*) and interlobular septal thickening (*curved arrows*). GGO and dependent atelectasis at left base creates false appearance of bronchiectasis.

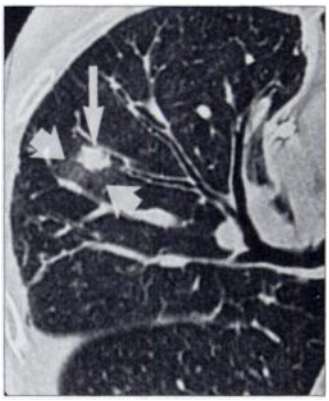

Fig. 10.—62-year-old woman with postbiopsy nodule 3 months after right lung transplantation. High-resolution CT scan obtained 1 week after right upper lobe biopsy shows nodular opacity (*long arrow*) with surrounding halo of ground-glass opacity (*short arrows*), representing postbiopsy hemorrhage. Histology showed no evidence of infection or rejection, and nodule resolved without treatment, as shown on follow-up CT scan 2 months later.

Fig. 11.—50-year-old man with bronchiolitis obliterans and worsening pulmonary function tests 17 months after bilateral lung transplantation. High-resolution CT scan shows ground-glass opacity with airway distribution on left (*long arrows*), peripheral distribution on right, and bronchiolectasis (*short arrows*). Transbronchial biopsy confirmed diagnosis of bronchiolitis obliterans and mild interstitial fibrosis, but no acute rejection or infection was diagnosed. Bronchiolitis obliterans in this patient population represents chronic rejection.

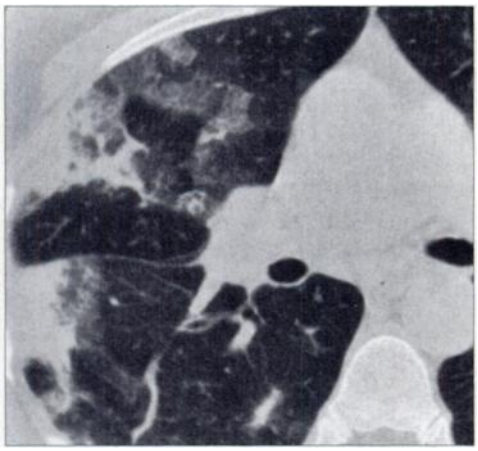

Fig. 12.—69-year-old woman who developed acute respiratory failure caused by bronchiolitis obliterans organizing pneumonia. High-resolution CT scan shows focal areas of consolidation and ground-glass opacity in peripheral distribution involving only right lung.

most patients in days or weeks, but some patients will have persistent disease, some patients will die, and approximately one third of patients will relapse on withdrawal of treatment. Nishimura and Itoh [35] compared the HRCT and open lung biopsy findings of eight patients with BOOP. HRCT scans showed sharply demarcated areas of consolidation or GGO in a panlobular distribution. Histologically, the GGO represented alveolar septal inflammation and alveolar cellular desquamation with a little granulation tissue in the terminal air space. In some of the specimens, interlobular septa or pulmonary veins formed a boundary, accounting for the presence of a sharp margin and panlobular distribution seen on HRCT. These authors also reported that in their experience BOOP is often indistinguishable radiographically and clinically from chronic eosinophilic pneumonia, although the diagnosis of eosinophilic pneumonia can be suggested with eosinophilia in the blood or bronchoalveolar lavage fluid. Müller and Miller [10] suggested that the major CT feature of BOOP is a ground-glass pattern with a predominantly subpleural distribution in about half the cases. CT and HRCT findings in patients with BOOP include GGO (seen in 8–75% of patients), nodules, or areas of consolidation with a predominant peripheral, bilateral, and nonsegmental distribution [36–38].

Bronchoalveolar lavage.—Bronchoalveolar lavage is a procedure used to diagnose pulmonary diseases and is used by pulmonary investigators studying the pathogenesis of disease in an attempt to improve diagnosis and identify predictors of prognosis. The recommended technique involves injection of 100–300 ml of normal saline (in 20 ml aliquots) through a bronchoscope wedged into the lingular or middle lobe bronchus. Fluid is then aspirated back into the scope and sent to the laboratory, where inflammatory and immune mediator cells are identified and counted and specific proteins are analyzed [39]. A segmental or lobar distribution of GGO on HRCT should suggest the possibility of recent bronchoalveolar lavage, especially if observed in the right middle lobe [3].

Bronchiolitis-associated interstitial lung disease.—Respiratory bronchiolitis-associated interstitial lung disease (RB-ILD) is a diagnosis based on the combination of clinical evidence of interstitial lung disease and restrictive pulmonary function abnormalities and respiratory bronchiolitis shown on lung biopsy. All reported cases have occurred in cigarette smokers [40–42]. Holt et al. [43] described the HRCT findings in five patients with biopsy-proven RB-ILD. HRCT scans of three of the five patients showed GGO that was extensive and that constituted the predominant finding in two patients. Other abnormalities included atelectasis, intralobular and interlobular interstitial thickening, and emphysema. These researchers concluded from their small series that GGO or coarse bands of atelectasis may be the only detectable pulmonary abnormalities on HRCT scans in patients with RB-ILD. Histopathologic findings consisted of pigmented macrophages arranged in a bronchiolocentric distribution within respiratory bronchioles and adjacent alveolar ducts and alveoli; and alveolar septa in involved areas often showed infiltration with chronic inflammatory cells, minimal fibrosis, and hyperplasia of alveolar lining cells. RB-ILD resembles desquamative interstitial pneumonitis pathologically but can be distinguished from that disease on the basis of the distribution of inflammatory changes at the bronchiolar and alveolar level [40]. In RB-ILD the abnormalities are patchy, and in desquamative interstitial pneumonitis they are more extensive and diffuse.

C

CMV pneumonia and other infections.—Infectious pneumonia of any cause can manifest as GGO on HRCT scans (Fig. 13), but CMV pneumonia and *Pneumocystis carinii* pneumonia are often emphasized. CMV is recognized as the most common viral pathogen to cause substantial morbidity and mortality in patients with AIDS; in autopsy studies, 49–81% of patients with AIDS have evidence of CMV infection [44, 45]. CMV pneumonia is also a relatively common complication in organ transplant recipients that can lead to respiratory failure and death (Fig. 14). McGuinness et al. [46] retrospectively evaluated CT scans, bronchoalveolar lavage, and biopsy results of 21 patients with AIDS and cytopathologic evidence of CMV infection without other infections. CT findings included GGO (nine of 21 patients), dense consolidation, bronchial wall thickening or bronchiectasis, and interstitial reticulation without air-space disease. Of the five patients with GGO on CT scans for whom pathology specimens were available, all showed air-space filling histologically. The air-space filling constituted a mixture of alveolar macrophages, fibrin, hyaline membranes, proliferating reactive and

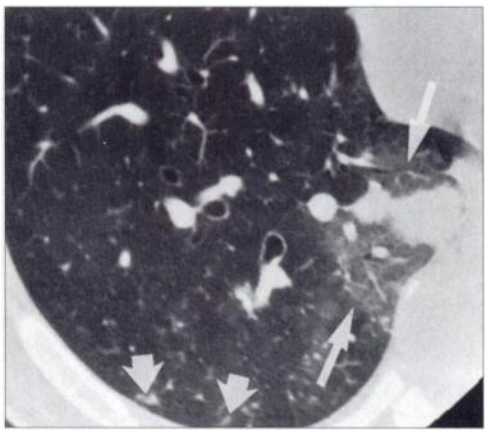

Fig. 13.—33-year-old man with hemoptysis caused by blastomycosis. High-resolution CT scan shows focal consolidation with surrounding ground-glass opacity in medial segment of right lower lobe (*long arrows*) and smaller foci of nodular and branching opacities peripherally (*short arrows*), consistent with endobronchial spread of blastomycosis.

Fig. 14.—42-year-old-man with cytomegalovirus (CMV) pneumonia who underwent ablative chemotherapy, total body irradiation, and allogeneic bone marrow transplantation for acute myelogenous leukemia. High-resolution CT (HRCT) scans and lung biopsy were performed 3 days after transplantation when patient developed acute respiratory symptoms. HRCT scan shows bilateral patchy areas of ground-glass opacity and bronchiolar dilatation. Histology revealed interstitial pneumonitis and CMV infection.

sloughed pneumonocytes, and old hemorrhage. In another study, Aafedt et al. [47] described the CT findings of CMV pneumonia in a population of non-AIDS patients and reported the most frequent CT appearance to be a mixed alveolar and interstitial pattern with some peripheral predominance. More recently, Kang et al. [48] studied 10 organ transplant patients who underwent chest CT and who had pathologically proven CMV pneumonia without other associated infections. Those authors reported the CT findings to be heterogeneous, consisting of small nodules, consolidation, GGO (four patients), and irregular lines. Histologically, the GGO represented early changes of diffuse alveolar damage. Because HRCT was performed in only three of the patients (conventional CT in the other seven), the presence of GGO may have been underestimated.

P. carinii *pneumonia.—P. carinii* pneumonia is another common pathogen in the immunocompromised host (Fig. 15). Kuhlman et al. [49] reviewed the CT findings in 39 patients with *P. carinii* pneumonia and reported three patterns of involvement: GGO (26%), a patchwork pattern consisting of mixed interstitial and alveolar disease (56%), and an interstitial pattern (18%). In another report, Sider et al. [50] studied chest CT scans of patients with AIDS and reported that the presence of an isolated ground-glass infiltrate without additional findings in the proper clinical setting was highly suggestive of *P. carinii* pneumonia. Bergin et al. [51] examined the HRCT scans of 14 immunocompromised patients with histologic proof of *P. carinii* pneumonia; all showed GGO. Two histologic features accounted for the GGO: fluid within alveoli that was foamy in appearance on microscopy and that was known to consist of surfactant, fibrin, and cellular debris; and thickening of the alveolar interstitium by edema and cellular infiltrates.

Cancer and lymphoproliferative disorders.—Most primary lung neoplasms consist of masslike areas of consolidation, with or without cavitation. Bronchioloalveolar carcinoma, a type of bronchogenic adenocarcinoma, most commonly presents as a solitary peripheral nodule but can also present as a focal area of GGO on HRCT scans [52] (Fig. 16). Such an area of GGO reflects the unique lepidic growth pattern of bronchioloalveolar carcinoma along the alveolar septa with relative lack of acinar filling. Follow-up CT scans in three of four patients with bronchioloalveolar carcinoma showed replacement of the GGO by consolidation, leading to speculation that the areas of GGO may represent an early stage of bronchioloalveolar carcinoma [52]. Metastatic adenocarcinoma can have a lepidic pattern of growth along intact alveolar walls similar to that of bronchioloalveolar carcinoma. Gaeta et al. [53] retrospectively reviewed CT scans of 65 patients with proven lung metastasis from gastrointestinal carcinomas. Six of 65 patients had air-space disease, and five of these six patients showed evidence of GGO. Bronchioloalveolar adenoma of the lung is considered histopathologically to be a highly differentiated adenocarcinoma or potentially malignant benign neoplasm and is usually discovered incidentally at microscopic examination of surgically resected lung specimens [54]. Kushihashi et al. [55] studied the CT scans of 668 patients with lung cancer and found nine small ground-glass nodules, seven of which were subsequently shown to represent bronchioloalveolar adenoma. These researchers concluded that in a patient with known lung carcinoma, a focal small nodule of GGO must be investigated to rule out bronchioloalveolar adenoma or multicentric adenocarcinoma.

Intrathoracic lymphoproliferative disorders, seen predominantly in patients with AIDS and other immunodeficiences, range from benign lymphoid cell hyperplasia to malignant lymphoma. Carignan et al. [56] studied the chest CT scans of 12 patients with pathologically proven lymphoproliferative disorders (AIDS-related diffuse lymphoid hyperplasia, lymphocytic interstitial pneumonia, posttransplantation lymphoproliferative disorders, and lymphoma) and found diffuse areas of GGO in the patient with lymphoid hyperplasia and the three patients with lymphocytic interstitial pneumonia. Three of the four patients with posttransplantation lymphoproliferative disorders had multiple, well-circumscribed pulmonary nodules with a halo of GGO. Histologically, the halo was found to represent less densely arranged B cells that extended into the surrounding interstitium. The predominant finding in two patients with AIDS-related lymphocytic interstitial pneumonia was the presence of diffuse bilateral areas of GGO histologically representing a diffuse interstitial lymphocytic infiltrate. Another study comparing the chest CT and histopathologic findings in nine patients with HIV infection or AIDS and lymphoproliferative disorders found 2- to 4-mm nodules to be the predominant CT finding [57]. Only one patient had evidence of GGO without nodules, which histologically represented a nodular pattern of interstitial lymphocytic infiltrate.

Collagen vascular disease.—Collagen vascular disease is a chronic multisystem dis-

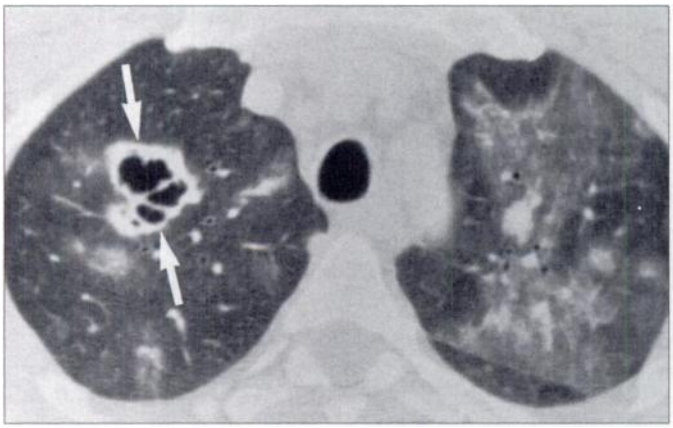

Fig. 15.—39-year-old man with AIDS and *Pneumocystis carinii* pneumonia. High-resolution CT scan shows multiseptated cavitary lesion in right upper lobe (*arrows*) and patchy ground-glass opacity bilaterally.

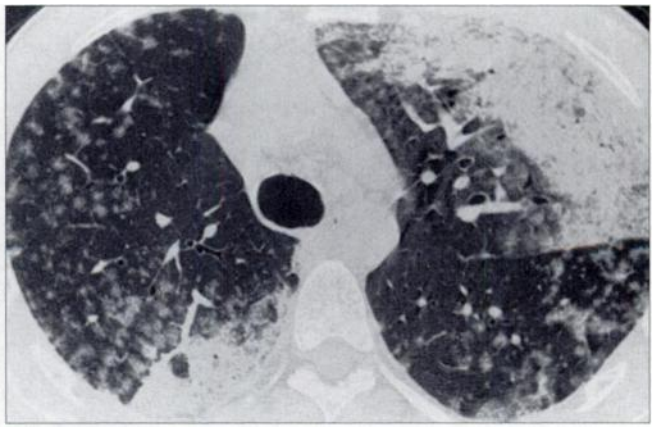

Fig. 16.—60-year-old man with bronchioloalveolar cell carcinoma. CT scan shows bilateral patchy lung disease most pronounced in right lower lobe and left upper lobe. Note multiple ill-defined nodular areas of ground-glass opacity scattered throughout lungs around pulmonary centrilobular-sized bronchioles. Anterior portion of lingula is densely opacified.

ease characterized by vascular changes, fibrosis, and inflammation of connective tissue. All types may involve the respiratory system. Specific abnormalities of the lung associated with collagen vascular diseases include usual interstitial pneumonia, diffuse alveolar damage, BOOP, cellular interstitial pneumonia, and lymphocytic interstitial pneumonia. Johkoh et al. [58] evaluated HRCT scans and pulmonary function tests in 55 patients with collagen vascular disease, including progressive systemic sclerosis, systemic lupus erythematosus, polymyositis and dermatomyositis, rheumatoid arthritis, and Sjögren's syndrome, and compared the findings with those of nine patients with idiopathic pulmonary fibrosis. GGO was seen in 89% of patients with progressive systemic sclerosis, 100% with systemic lupus erythematosus, 71% with polymyositis and dermatomyositis, 100% with rheumatoid arthritis, and 63% with Sjögren's syndrome. The incidence of GGO in idiopathic pulmonary fibrosis was the same as in collagen vascular disease; but with the exception of progressive systemic sclerosis, the incidence of associated honeycombing was significantly lower in collagen vascular disease than in idiopathic pulmonary fibrosis. Remy-Jardin et al. [59] reported the HRCT findings of 77 patients with rheumatoid arthritis. Thirty-eight patients (49%) had CT scans showing bronchiectasis or bronchiolectasis (30%), pulmonary nodules (22%), subpleural micronodules or pseudoplaques (17%), nonseptal linear attenuation (18%), areas of GGO (14%), and honeycombing (10%).

Contusion.—Pulmonary contusion, a condition implying bleeding into the air spaces and interstitium of the lung without major disruption of lung architecture, is generally accepted as the primary lung injury following blunt chest trauma. Pulmonary contusion is usually caused by a compression injury adjacent to the site of chest wall injury, resulting in a peripheral distribution of lung opacity. The CT appearance of lung contusion is that of ill-defined areas of GGO or consolidation without segmental distribution but usually with a peripheral distribution [60, 61]. In experimentally induced contusions, Schild et al. [62] showed that CT was superior to chest radiography in detecting pulmonary contusions. In their study, 100% of pulmonary contusions were visible on CT immediately after trauma, suggesting that pulmonary contusion is unlikely in a trauma patient whose CT scan shows normal findings. Most pulmonary contusions start to resolve within 72 hrs and clear in 10–14 days without CT or radiographic sequelae (Fig. 17).

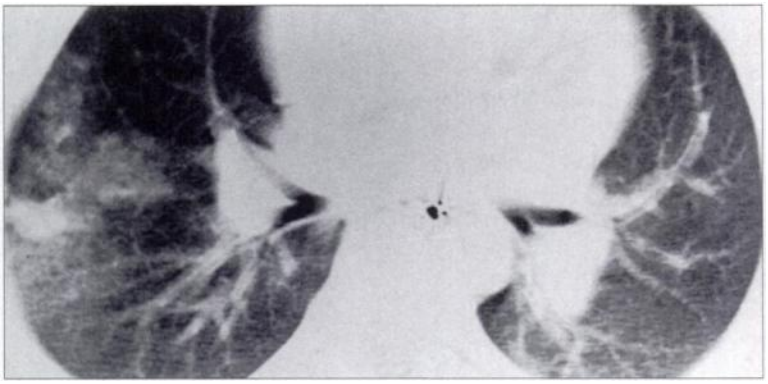

Fig. 17.—12-year-old boy who developed pulmonary contusion after motor vehicle accident. CT scan of chest shows ill-defined nonanatomic peripheral areas of ground-glass opacity and consolidation. No evidence is seen of underlying pulmonary laceration or other intrathoracic injury.

D

Drug toxicity.—Pulmonary toxicity has been associated with numerous drugs, and a variety of pathophysiologic mechanisms producing lung injury results in varying radiographic and CT patterns. Early recognition of drug toxicity may allow reversal of the lung injury with withdrawal of the inciting agent. Aronchick and Gefter [63] reported on the common radiographic patterns of specific drug toxicities, including diffuse alveolar opacities, diffuse interstitial opacities, focal alveolar opacities, and pulmonary nodules. The list of inciting agents is long, and many drugs can produce more than one pattern of parenchymal disease, but representative CT scans show nodular areas of GGO and consolidation, often with a peripheral distribution. Typical and unique features of amiodarone (an iodinated compound used to treat life-threatening ventricular dysrhythmias) lung toxicity are pleural-based wedge-shaped high-attenuation areas of consolidation or focal atelectasis adjacent to the pleura. The high attenuation in these lesions is due to the concentration of iodine in the lung parenchyma. Bleomycin, a chemotherapeutic agent used routinely in treating lymphoma and seminomatous and nonseminomatous germ cell tumors of the testes, has also been reported to produce pulmonary toxicity, which on CT manifests as pleural-based linear and nodular GGO or consolidated irregularities [64]. Patz et al. [65] retrospectively evaluated the CT findings in 20 patients with pulmonary drug toxicity that followed high-dose chemotherapy and autologous bone marrow transplantation. CT scans of 13 patients (65%) showed scattered, predominantly peripheral ground-glass or consolidated opacities that occasionally looked nodular or masslike.

Desquamative interstitial pneumonitis.—Desquamative interstitial pneumonitis was first described by Liebow et al. [66] in 1965, who characterized the condition by the presence of relatively mild respiratory symptoms, mild fibrosis of alveolar septa, and a cellular infiltrate in the alveolar air spaces (now known to be macrophages). Hartman et al. [67] reported on the HRCT findings of 22 patients with pathologically proven desquamative interstitial pneumonitis. All 22 patients had areas of GGO on HRCT, with a lower lung zone (73%) and peripheral (59%) distribution predominating. Reticular lines, cysts, and traction bronchiectasis were less frequently seen findings. The predominant histologic lesion was filling of the alveoli with macrophages. Desquamative interstitial pneumonitis is a distinct form of interstitial pneumonia characterized by a more benign clinical course than usual interstitial pneumonia. Other interstitial pneumonias (lymphocytic interstitial pneumonia, giant cell interstitial pneumonia, bronchiolitis obliterans interstitial pneumonia), as classified by Liebow et al. [66], can show similar radiographic features. Primack et al. [68] described the HRCT features in nine patients with biopsy- or autopsy-proven acute interstitial pneumonitis, an entity variously known as Hamman-Rich syndrome, accelerated interstitial pneumonia, and diffuse alveolar damage. Bilateral symmetric areas of GGO were present on the CT scans of all nine patients, which correlated histologically with thickening of the interstitium by inflammatory cells, fibroblast proliferation, and edema, with evidence of diffuse alveolar damage and hyaline membrane formation. Park et al. [69] described the HRCT findings in seven patients

with pathologically proven nonspecific interstitial pneumonia, a distinct clinical and pathologic entity of idiopathic interstitial pneumonia (distinct from acute interstitial pneumonitis, desquamative interstitial pneumonitis, and usual interstitial pneumonia), which manifests with subacute or chronic dyspnea and has a good prognosis with corticosteroid therapy. These researchers found the most common HRCT findings to be bilateral patchy areas of GGO with or without consolidation that correlated histologically with interstitial inflammation and fibrosis.

E

Extrinsic allergic alveolitis.—Extrinsic allergic alveolitis or hypersensitivity pneumonitis is a complex immunologic reaction by the lung, primarily to inhaled organic antigens, although noninhaled drugs can also be an inciting agent. The most important and common disorders and their inciting agents are farmer's lung from thermophilic actinomycetes in moldy hay (Fig. 18), bagassosis from *Thermoactinomyces sacchari* in moldy sugar cane, mushroom worker's lung from thermophilic actinomycetes in mushroom compost, ventilation pneumonitis from *T. vulgaris* (among others) in dust or mist, malt worker's lung from *Aspergillus clavatus* in moldy barley, and bird fancier's (breeder's) lung from avian protein in droppings and feathers [70]. The clinical presentation may be categorized as acute, subacute, or chronic, depending on the periodicity of exposure and the quantity of inhaled antigen. Hansell et al. [71] correlated the pattern and extent of abnormalities seen on HRCT scans with pulmonary function test results in 22 patients with subacute and chronic hypersensitivity pneumonitis. The most common HRCT patterns were decreased attenuation and mosaic perfusion (86%), GGO (82%), small nodules (55%), and a reticular pattern (36%). Areas of decreased attenuation correlated with severity of air trapping indicated by residual volume, whereas GGO and reticulation correlated independently with restrictive lung function. Hansell et al. concluded that GGO, although seen in many other diffuse lung diseases, is a dominant feature in subacute hypersensitivity pneumonitis, correlating pathologically with mononuclear cell infiltration of the alveolar walls. In another study attempting to establish whether CT can distinguish hypersensitivity pneumonitis from idiopathic pulmonary fibrosis, HRCT scans showed widespread GGO in patients with idiopathic pulmonary fibrosis and desquamative interstitial pneumonia, indistinguishable from some cases of acute or subacute hypersensitivity pneumonitis [72]. Akira et al. [73] studied the HRCT scans of 15 patients with summer-type hypersensitivity pneumonitis, an immunologic disease occurring only in Japan in which the clinical symptoms appear in the summer and subside spontaneously in mid autumn. HRCT findings included diffuse micronodules (100%), slightly elevated lung density or GGO (87%), and patchy air-space consolidation (87%).

Eosinophilic pneumonia.—Pulmonary eosinophilia occurs in a variety of conditions or diseases such as bronchopulmonary aspergillosis; bronchocentric granulomatosis; pulmonary infections including bacterial, fungal, and helminth infections; idiopathic pulmonary fibrosis; sarcoidosis; collagen vascular diseases; hypereosinophilic syndrome; Churg-Strauss syndrome; Hodgkin's disease; and drug reactions [74]. When these underlying diseases or specific causes are excluded, pulmonary eosinophilia is classified as idiopathic, either acute or chronic. Chronic eosinophilic pneumonia is characterized by multiple dense areas of opacity on chest radiographs and CT scans, persistent clinical course, rapid improvement with steroid therapy, and possible relapse. In contrast, acute eosinophilic pneumonia is characterized by diffuse GGO and micronodules on chest radiographs and CT scans, acute onset with high fever, spontaneous improvement during hospitalization, rapid improvement if treated with steroids, and no relapse (Fig. 19). The appearance of acute eosinophilic pneumonia on HRCT has been described as peripheral GGO along the bronchovascular bundles correlating histologically with edematous interstitial tissues with scattered eosinophil infiltration and no alveolar filling [75]. In a study of 17 patients with pathologically proven or clinically diagnosed chronic eosinophilic pneumonia, the most common HRCT finding was GGO, usually adjacent to areas of consolidation, with a

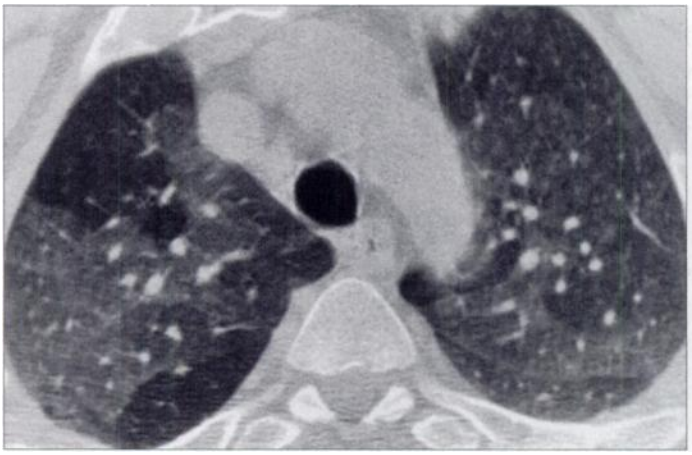

Fig. 18.—50-year-old farmer with 3-month history of cough and shortness of breath resulting from hypersensitivity pneumonitis. High-resolution CT scan shows patchy areas of ground-glass opacity, correlating with clinical and histologic diagnosis of acute hypersensitivity pneumonitis (farmer's lung).

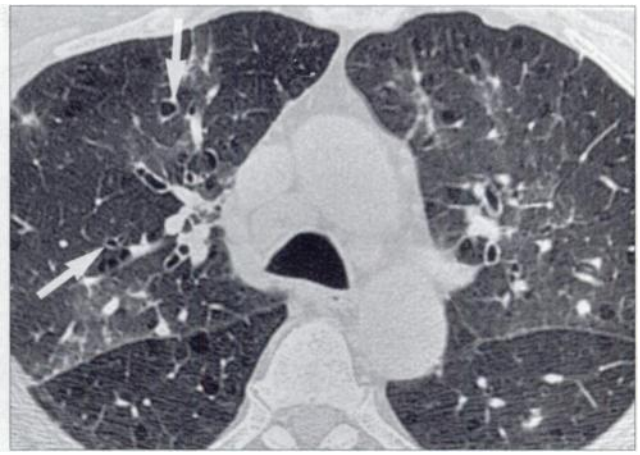

Fig. 19.—71-year-old man with acute onset of wheezing, shortness of breath, and fever resulting from acute eosinophilic pneumonia. Eosinophil count was markedly elevated in bronchoalveolar lavage fluid and in peripheral blood, and patient's symptoms resolved with steroid treatment. Before steroid treatment, patient had no improvement in symptoms with bronchodilators. High-resolution CT (HRCT) scan shows bilateral patchy ground-glass opacity in bronchovascular distribution and airway dilatation (*arrows*). Airway dilatation resolved on follow-up HRCT. Extensive workup revealed no evidence of primary cause of eosinophilic pneumonia.

peripheral distribution [76]. Histologic studies of chronic eosinophilic pneumonia show an intraalveolar exudate of eosinophils, histiocytes and, occasionally, amorphous material, and eosinophilic interstitial infiltration [77].

Edema.—Cardiogenic pulmonary edema is the consequence of high pulmonary capillary and venous pressure due to failure of the left side of the heart, with edema fluid collecting in the alveolar spaces, interstitial spaces, or a combination of the two. Identical CT findings can be found in pulmonary edema of cardiac or noncardiac origin. Edema can occur in all situations in which the capacity of the lung lymphatics to drain capillary transudate is exceeded, including venous and lymphatic obstruction, increased capillary permeability, and hypoproteinemia [3]. Storto et al. [78] described the HRCT findings of seven patients thought to have lung disease who subsequently had a diagnosis of hydrostatic pulmonary edema on the basis of clinical history and the resolution of abnormalities on radiology after therapy with diuretics. Abnormalities visible on HRCT scans included areas of GGO (six patients), interlobular septal thickening (five patients), peribronchovascular interstitial thickening (five patients), increased vascular caliber (four patients), and pleural effusion or thickening of fissures (four patients). The GGO can appear diffuse or patchy and geographic, often with a gravitational predominance that is thought to represent minimal thickening of the pulmonary interstitium, intraalveolar fluid layering against the alveolar walls, or a transient increase in the pulmonary capillary blood volume (Fig. 20).

F and G

Fibrosis.—GGO can be a reflection of extensive lung parenchymal fibrosis with minimal alveolitis [3]. To evaluate the prognostic implications of GGO at HRCT in assessing response to treatment of fibrosing alveolitis, Lee et al. [79] correlated HRCT findings with the improvement in pulmonary function as represented by the increase in percentage-predicted values on pulmonary function tests after corticosteroid therapy. These researchers found that the presence of GGO at HRCT is a good predictor of response to treatment in fibrosing alveolitis. Subsequently, Remy-Jardin et al. [80] studied 26 patients with chronic diffuse lung disease (desquamative interstitial pneumonitis, usual interstitial pneumonitis, sarcoidosis, BOOP, hypersensitivity pneumonitis, and scleroderma) who had extensive areas of GGO as the predominant or exclusive abnormality at HRCT in the absence of honeycombing. In this patient group, areas of GGO were found to be a reliable indicator of inflammation, but only in the absence of signs of fibrosis such as bronchiectasis or honeycombing. Retrospective assessment of disease activity remains possible on follow-up CT scans when decreased or complete resolution of GGO is observed.

Conversely, persistence of GGO after steroid treatment indicates fibrosis (Fig. 21). When follow-up CT scans show sequential replacement of GGO by typical honeycombing, the initial CT findings may correspond to pathologic changes observed in the acute phase of lung injury or they may be due to partial volume averaging with thickened interstitial tissue or a microcystic honeycomb pattern on HRCT [3]. Like Remy-Jardin et al. [80], Wells et al. [81] found that the prognostic significance of GGO on CT depends on the extent of an associated reticular pattern and is independent of the extent and distribution of disease. Furthermore, fine intralobular fibrosis, which lies below the limits of resolution of the CT scanner, may not be depicted as a reticular abnormality but might result in an amorphous increase in lung density because of volume averaging. Hartman et al. [82] studied 12 patients with usual interstitial pneumonitis and 11 patients with desquamative interstitial pneumonitis who had initial and follow-up HRCT and found that in patients with usual interstitial pneumonitis, areas of GGO usually increase in extent or progress to fibrosis despite treatment, and areas of GGO in most patients with desquamative interstitial pneumonitis remain stable or improve with treatment.

Granulomatous disease.—Many granulomatous diseases are known. This review will focus on sarcoidosis, one of the most common disorders in this class of diseases. Sarcoidosis is a multisystemic disorder of unknown cause characterized by the presence of noncaseating granulomatous inflammation that can affect various sites of the body, with a propensity to involve the respiratory tract (Figs. 22–24). The cellular and granulomatous elements of inflammation indicate activity, reversibility, and favorable response to medical treatment, whereas a fibrotic component indicates irreversibility and poor response to therapy. Nishimura et al. [83] correlated HRCT and histopathologic findings in eight

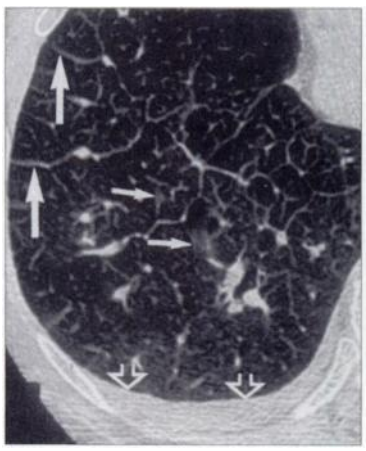

Fig. 20.—69-year-old woman with clinical and radiographic signs of cardiogenic edema, both of which resolved with diuretic therapy. High-resolution CT scan shows interlobular septal thickening (*large arrows*), patchy areas of ground-glass opacity (*small arrows*), and right pleural effusion (*open arrows*).

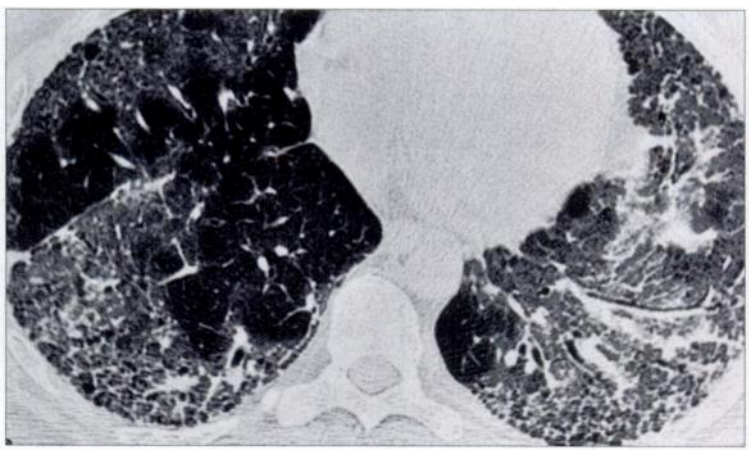

Fig. 21.—42-year-old-man with chronic progressive respiratory failure caused by idiopathic pulmonary fibrosis. High-resolution CT (HRCT) scan shows peripheral honeycombing and ground-glass opacity (GGO) bilaterally. GGO persisted on HRCT after treatment with steroids, consistent with fibrosis beyond resolution of CT scanner.

Fig. 22.—46-year-old woman with sarcoidosis and signs and symptoms of weight loss, shortness of breath, and cough. High-resolution CT scan shows bilateral areas of ground-glass opacity and airway dilatation radiating from hila to periphery of both lungs, with distribution along bronchovascular bundles. Right upper lobe transbronchial biopsy showed multiple noncaseating granulomas typical of sarcoidosis.

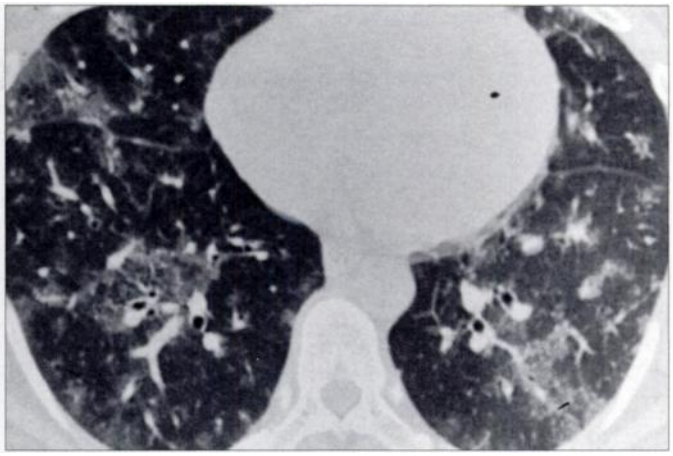

Fig. 23.—34-year-old woman with sarcoidosis. CT scan shows bilateral patchy areas of ground-glass opacity, correlating with histologic diagnosis of sarcoidosis.

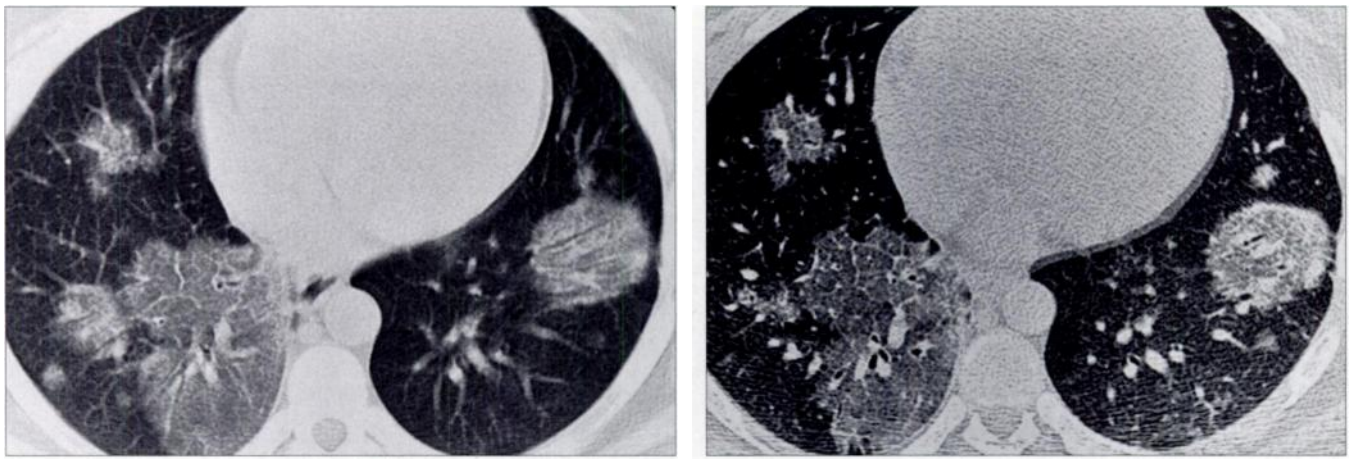

A **B**

Fig. 24.—25-year-old asymptomatic man with sarcoidosis.
A and **B**, Conventional (**A**) and high-resolution (**B**) CT scans show patchy bilateral areas of ground-glass opacity. Underlying reticular pattern is easier to appreciate on **B**.

patients with pulmonary sarcoidosis. The most frequent CT features were irregularly thickened bronchovascular bundles (88%) and small nodules along vessels (50%). These features corresponded to granulomas formed in the connective-tissue sheath around the pulmonary vessels and airways. GGO was present in six patients (75%), which correlated histologically with many granulomatous lesions, with or without perigranulomatous fibrosis, in the interstitium and alveolar septa and around small vessels. Active alveolitis could not be confirmed in lung specimens of any of the patients, including lung specimens obtained from areas showing GGO. Remy-Jardin et al. [84] investigated the role of HRCT in determining disease activity and functional impairment and in predicting the prognosis of lung involvement in patients with sarcoidosis. As many as 32% of patients had areas of GGO on HRCT, and no correlation was noted between GGO and disease activity. GGO in this patient population could correspond to granulomas and inflammatory infiltrates or to mild fibrosis. HRCT findings in three cases of pulmonary talcosis, a foreign body granulomatous reaction after IV injection of talc-containing drugs, have been reported by Padley et al. [85]. In one of their cases, HRCT showed widespread GGO, thought to represent small granulomatous nodules.

Conclusion

GGO is a nonspecific finding on chest CT scans and has been shown histologically to correlate with partial filling of air spaces, inflammatory or fibrotic interstitial thickening, and increased capillary blood volume. Numerous processes can result in GGO as the sole or dominant finding on chest CT scans; however, correlating the clinical history with the CT distribution of disease and any associated CT findings can lead to the correct diagnosis or at least narrow the range of diagnostic possibilities. Our classification scheme allows making a diagnosis from GGO on chest CT scans as easy as the ABCs.

For example, correlating GGO in a patient with a temporal history of antigenic exposure to inhaled organic dusts and appropriate clinical symptoms suggests the diagnosis of extrinsic allergic alveolitis. Systemic manifestations or a known history of a particular collagen vascular disease can strongly sug-

gest this diagnosis as the cause of GGO. GGO may be the predominant finding on CT scans in cigarette smokers with clinical symptoms of interstitial lung disease (RB-ILD). Hemorrhage is a consideration in a patient with a known history of a pulmonary–renal syndrome who has multifocal or diffuse areas of GGO on CT. In a patient with sickle cell disease and an acute onset of fever and chest pain, acute chest syndrome is the probable diagnosis when the CT scan shows areas of GGO. A pattern of predominantly diffuse GGO on CT scans suggests diffuse alveolar hemorrhage in patients with leukemia, *P. carinii* in patients with AIDS, and acute rejection or CMV pneumonia in immunosuppressed patients after lung transplantation. Focal areas of GGO surrounding dense nodules strongly suggest invasive pulmonary aspergillosis in patients with leukemia, postbiopsy nodules in patients after lung transplantation, and lymphoproliferative disease in immunocompromised patients.

The CT scan distribution of GGO is helpful in narrowing the range of diagnostic possibilities. A peripheral distribution of GGO on CT scans suggests pulmonary contusion when a history exists of blunt trauma to the chest wall. Without a history of recent trauma, a peripheral distribution of GGO on CT scans suggests the diagnosis of eosinophilic pneumonia, BOOP, sarcoidosis, or drug toxicity. Each of these has different clinical presentations or associated CT findings. For example, CT scans in patients with sarcoidosis can show nodules in a bronchovascular distribution and mediastinal and hilar adenopathy. A bibasilar and subpleural distribution of GGO on CT scans is characteristic of the distribution for usual interstitial pneumonitis, desquamative interstitial pneumonitis, and other interstitial pneumonias. Isolated right middle lobe GGO on a CT scan can be explained by residual fluid from bronchoalveolar lavage with the appropriate history. Solitary small areas of GGO can signify early stage bronchioloalveolar carcinoma, or bronchioloalveolar adenoma in a patient with a known lung cancer.

Associated CT findings help to narrow the differential diagnosis when GGO is present. Underlying reticular lines forming polygonal forms, or "crazy paving," is suggestive of pulmonary alveolar proteinosis. The combination of increased vessel caliber and heart size, pleural effusions, septal thickening, and GGO with a gravitational predominance supports the diagnosis of pulmonary edema. GGO associated with traction bronchiectasis and honeycombing indicates pulmonary fibrosis. Features of barotrauma, such as interstitial pulmonary emphysema, pneumothorax, pneumomediastinum, and pneumatoceles are seen in patients with ARDS, although the initial CT finding in this patient population may be GGO and consolidation.

References

1. Austin JHM, Müller NL, Friedman PJ, et al. Glossary of terms for CT of the lungs: recommendations of the Nomenclature Committee of the Fleischner Society. *Radiology* **1996**;200:327–331
2. Klein JS, Gamsu G. High-resolution computed tomography of diffuse lung disease. *Invest Radiol* **1989**;24:805–812
3. Remy-Jardin M, Remy J, Giraud F, Wattinne L, Gosselin B. Computed tomography assessment of ground-glass opacity: semiology and significance. *J Thorac Imaging* **1993**;8:249–264
4. Engeler CE, Tashjian JH, Trenkner SW, Walsh JW. Ground-glass opacity of the lung parenchyma: a guide to analysis with high-resolution CT. *AJR* **1993**;160:249–251
5. Webb WR, Müller NL, Naidich DP. *High-resolution CT of the lung*, 2nd ed. Philadelphia: Lippincott-Raven, **1996**
6. Bessis L, Callard P, Gotheil C, Biaggi A, Grenier P. High-resolution CT of parenchymal lung disease: precise correlation with histologic findings. *RadioGraphics* **1992**;12:45–58
7. Corcoran HL, Renner WR, Milstein MJ. Review of high-resolution CT of the lung. *RadioGraphics* **1992**;12:917–939
8. Swensen SJ, Aughenbaugh GL, Douglas WW, Myers JL. High-resolution CT of the lungs: findings in various pulmonary diseases. *AJR* **1992**;158:971–979
9. Müller NL, Miller RR. State of the art: computed tomography of chronic diffuse infiltrative lung disease, part 1. *Am Rev Respir Dis* **1990**;142:1206–1215
10. Müller NL, Miller RR. State of the art: computed tomography of chronic diffuse infiltrative lung disease, part 2. *Am Rev Respir Dis* **1990**;142:1440–1448
11. Aberle DR. HRCT in acute diffuse lung disease. *J Thorac Imaging* **1993**;8:200–212
12. Stern EJ, Swensen SJ, Hartman TE, Frank MS. CT mosaic pattern of lung attenuation: distinguishing different causes. *AJR* **1995**;165:813–816
13. Primack SL, Remy-Jardin M, Remy J, Müller NL. High-resolution CT of the lung: pitfalls in the diagnosis of infiltrative lung disease. *AJR* **1996**;167:413–418
14. Zwirewich CV, Mayo JR, Müller NL. Low-dose high-resolution CT of lung parenchyma. *Radiology* **1991**;180:413–417
15. Zerhouni EA, Naidich DP, Stitik FP, Khouri NF, Siegelman SS. Computed tomography of the pulmonary parenchyma. II. Interstitial disease. *J Thorac Imaging* **1985**;1:54–64
16. Mayo JR, Webb WR, Gould R, et al. High-resolution CT of the lungs: an optimal approach. *Radiology* **1987**;163:507–510
17. Rosen SH, Castleman B, Liebow AA. Pulmonary alveolar proteinosis. *N Engl J Med* **1958**;258:1123–1144
18. Nhieu JTV, Vojtek AM, Bernaudin JF, Escudier E, Fleury-Feith J. Pulmonary alveolar proteinosis associated with *Pneumocystis carinii*: ultrastructural identification in bronchoalveolar lavage in AIDS and immunocompromised non-AIDS patients. *Chest* **1990**;98:801–805
19. Godwin JD, Müller NL, Takasugi JE. Pulmonary alveolar proteinosis: CT findings. *Radiology* **1988**;169:609–613
20. Murch CR, Carr DH. Computed tomography appearances of pulmonary alveolar proteinosis. *Clin Radiol* **1989**;40:240–243
21. Barrett-Connor E. Pneumonia and pulmonary infection in sickle cell anemia. *JAMA* **1973**;224:997–1000
22. Haupt HM, Moore W, Bauer TW, et al. The lung in sickle cell disease. *Chest* **1982**;81:332–337
23. Bhalla M, Abboud MR, McLoud TC, et al. Acute chest syndrome in sickle cell disease: CT evidence of microvascular occlusion. *Radiology* **1993**;187:45–49
24. Loubeyre P, Revel D, Delignette A, Loire R, Mornex JF. High-resolution computed tomographic findings associated with histologically diagnosed acute lung rejection in heart-lung transplant recipients. *Chest* **1995**;107:132–138
25. Hansell DM, Peters AM. Pulmonary vascular diseases and pulmonary edema. In: Armstrong P, Dee P, Hansell DM, Keats TE, Peters AM, Wilson AG, eds. *Imaging of diseases of the chest*, 2nd ed. St. Louis: Mosby, **1995**:369–425
26. Tagliabue M, Casella TC, Zincone GE, Fumagalli R, Salvini E. CT and chest radiography in the evaluation of adult respiratory distress syndrome. *Acta Radiol* **1994**;35:230–234
27. Owens CM, Evans TW, Keogh BF, Hansell DM. Computed tomography in established adult respiratory distress syndrome: correlation with lung injury score. *Chest* **1994**;106:1815–1821
28. Albelda SM, Gefter WB, Epstein DM, Miller WT. Diffuse pulmonary hemorrhage: a review and classification. *Radiology* **1985**;154:289–297
29. Cheah FK, Sheppard MN, Hansell DM. Computed tomography of diffuse pulmonary haemorrhage with pathological correlation. *Clin Radiol* **1993**;48:89–93
30. Kuhlman JE, Fishman EK, Siegelman SS. Invasive pulmonary aspergillosis in acute leukemia: characteristic findings on CT, the CT halo sign, and the role of CT in early diagnosis. *Radiology* **1985**;157:611–614
31. Primack SL, Hartman TE, Lee KS, Müller NL. Pulmonary nodules and the CT halo sign. *Radiology* **1994**;190:513–515
32. Kazerooni EA, Cascade PN, Gross BH. Transplanted lungs: nodules following transbronchial biopsy. *Radiology* **1995**;194:209–212
33. Epler GR, Colby TV. The spectrum of bronchiolitis obliterans. *Chest* **1983**;83:161–162
34. Epler GR, Colby TV, McLoud TC, Carrington CB, Gaensler EA. Bronchiolitis obliterans organizing pneumonia. *N Engl J Med* **1985**;312:152–158
35. Nishimura K, Itoh H. High-resolution computed tomographic features of bronchiolitis obliterans organizing pneumonia. *Chest* **1992**;102:26S–31S
36. Logan PM, Miller RR, Müller NL. Cryptogenic organizing pneumonia in the immunocompro-

mised patient: radiologic findings and follow-up in 12 patients. *Can Assoc Radiol J* **1995**;46:272–279
37. Preidler KW, Szolar DM, Moelleken S, Tripp R, Schreyer H. Distribution pattern of computed tomography findings in patients with bronchiolitis obliterans organizing pneumonia. *Invest Radiol* **1996**;31:251–255
38. Bouchardy LM, Kuhlman JE, Ball WC, Hruban RH, Askin FB, Siegelman SS. CT findings in bronchiolitis obliterans organizing pneumonia (BOOP) with radiographic, clinical, and histologic correlation. *J Comput Assist Tomogr* **1993**;17:352–357
39. Methods of clinical, laboratory, and functional investigation. In: Fraser RS, Pare JAP, Fraser RG, Pare PD, eds. *Synopsis of diseases of the chest*, 2nd ed. Philadelphia: Saunders, **1994**:141–164
40. Myers JL, Veal CFJ, Shin MS, Katzenstein A-LA. Respiratory bronchiolitis causing interstitial lung disease: a clinicopathologic study of six cases. *Am Rev Respir Dis* **1987**;135:880–884
41. Yousem SA, Colby TV, Gaensler EA. Respiratory bronchiolitis-associated interstitial lung disease and its relationship to desquamative interstitial pneumonia. *Mayo Clin Proc* **1989**;64:1373–1380
42. Myers J. Respiratory bronchiolitis with interstitial lung disease. *Semin Respir Med* **1992**;13:134–139
43. Holt RM, Schmidt RA, Godwin JD, Raghu G. High-resolution CT in respiratory bronchiolitis-associated interstitial lung disease. *J Comput Assist Tomogr* **1993**;17:46–50
44. Wallace MJ, Hannah J. Cytomegalovirus pneumonitis in patients with AIDS: findings in an autopsy series. *Chest* **1987**;92:198–203
45. McKenzie R, Travis WD, Dolan SA, et al. The causes of death in patients with human immunodeficiency virus infection: a clinical and pathologic study with emphasis on the role of pulmonary diseases. *Medicine* **1991**;70:326–343
46. McGuinness G, Scholes JV, Garay SM, Leitman BS, McCauley DI, Naidich DP. Cytomegalovirus pneumonitis: spectrum of parenchymal CT findings with pathologic correlation in 21 AIDS patients. *Radiology* **1994**;192:451–459
47. Aafedt BC, Halvorsen RA, Tylen U, Hertz M. Cytomegalovirus pneumonia: computed tomography findings. *Can Assoc Radiol J* **1990**;41:276–280
48. Kang EY, Patz EF, Müller NL. Cytomegalovirus pneumonia in transplant patients: CT findings. *J Comput Assist Tomogr* **1996**;20:295–299
49. Kuhlman JE, Kavuru M, Fishman EK, Siegelman SS. *Pneumocystis carinii* pneumonia: spectrum of parenchymal CT findings. *Radiology* **1990**;175:711–714
50. Sider L, Gabriel H, Curry DR, Pham MS. Pattern recognition of the pulmonary manifestations of AIDS on CT scans. *RadioGraphics* **1993**;13:771–784
51. Bergin CJ, Wirth RL, Berry GJ, Castellino RA. *Pneumocystis carinii* pneumonia: CT and HRCT observations. *J Comput Assist Tomogr* **1990**;14:756–759
52. Jang HJ, Lee KS, Kwon OJ, Rhee CH, Shim YM, Han J. Bronchioloalveolar carcinoma: focal area of ground-glass attenuation at thin-section CT as an early sign. *Radiology* **1996**;199:485–488
53. Gaeta M, Volta S, Scribano E, Loria G, Vallone A, Pandolfo I. Air-space pattern in lung metastasis from adenocarcinoma of the GI tract. *J Comput Assist Tomogr* **1996**;20:300–304
54. Miller RR. Bronchioloalveolar cell adenomas. *Am J Surg Pathol* **1990**;14:904–912
55. Kushihashi T, Munechika H, Ri K, et al. Bronchioloalveolar adenoma of the lung: CT-pathologic correlation. *Radiology* **1994**;193:789–793
56. Carignan S, Staples CA, Müller NL. Intrathoracic lymphoproliferative disorders in the immunocompromised patient: CT findings. *Radiology* **1995**;197:53–58
57. McGuinness G, Scholes JV, Jagirdar JS, et al. Unusual lymphoproliferative disorders in nine adults with HIV or AIDS: CT and pathologic findings. *Radiology* **1995**;197:59–65
58. Johkoh T, Ikezoe J, Kohno N, et al. High-resolution CT and pulmonary function tests in collagen vascular disease: comparison with idiopathic pulmonary fibrosis. *Eur J Radiol* **1994**;18:113–121
59. Remy-Jardin M, Remy J, Cortet B, Mauri F, Delcambre B. Lung changes in rheumatoid arthritis: CT findings. *Radiology* **1994**;193:375–382
60. Wagner RB, Crawford WO, Schimpf PP. Classification of parenchymal injuries of the lung. *Radiology* **1988**;167:77–82
61. Schnyder P, Gamsu G, Essinger A, Duvoisin B. Trauma. In: Moss AA, Gamsu G, Genant HK, eds. *Computed tomography of the body*. Philadelphia: Saunders, **1992**:311–323
62. Schild HH, Strunk H, Weber W. Pulmonary contusion: CT vs plain radiograms. *J Comput Assist Tomogr* **1989**;13:417–420
63. Aronchick JM, Gefter WB. Drug-induced pulmonary disorders. *Semin Roentgenol* **1995**;30:18–34
64. Bellamy EA, Husband JE, Blaquiere RM, Law MR. Bleomycin-related lung damage: CT evidence. *Radiology* **1985**;156:155–158
65. Patz EF, Peters WP, Goodman PC. Pulmonary drug toxicity following high-dose chemotherapy with autologous bone marrow transplantation: CT findings in 20 cases. *J Thorac Imaging* **1994**;9:129–134
66. Liebow AA, Steer A, Billingsley JG. Desquamative interstitial pneumonia. *Am J Med* **1965**;38:369–404
67. Hartman TE, Primack SL, Swensen SJ, Hansell D, McGuinness G, Müller NL. Desquamative interstitial pneumonia: thin-section CT findings in 22 patients. *Radiology* **1993**;187:787–790
68. Primack SL, Hartman TE, Ikezoe J, Akira M, Sakatani M, Müller NL. Acute interstitial pneumonia: radiographic and CT findings in nine patients. *Radiology* **1993**;188:817–820
69. Park JS, Lee KS, Kim JS, et al. Nonspecific interstitial pneumonia with fibrosis: radiographic and CT findings in seven patients. *Radiology* **1995**;195:645–648
70. Wilson AG. Immunologic diseases of the lungs. In: Armstrong P, Wilson AG, Dee P, Hansell DM, eds. *Imaging of diseases of the chest*. St. Louis: Mosby, **1995**:485–567
71. Hansell DM, Wells AU, Padley SPG, Müller NL. Hypersensitivity pneumonitis: correlation of individual CT patterns with functional abnormalities. *Radiology* **1996**;199:123–128
72. Lynch DA, Newell JD, Logan PM, King TE Jr, Müller NL. Can CT distinguish hypersensitivity pneumonitis from idiopathic pulmonary fibrosis? *AJR* **1995**;165:807–811
73. Akira M, Kita N, Higashihara T, Sakatani M, Kozuka T. Summer-type hypersensitivity pneumonitis: comparison of high-resolution CT and plain radiographic findings. *AJR* **1992**;158:1223–1228
74. Hayakawa H, Sato A, Toyoshima M, Imokawa S, Taniguchi M. A clinical study of idiopathic eosinophilic pneumonia. *Chest* **1994**;105:1462–1466
75. Tsunemi K, Kanayama I, Kondo T, Tanigaki T, Ohta Y, Yanagimachi N. Acute eosinophilic pneumonia evaluated with high-resolution computed tomography. *Intern Med* **1993**;32:891–894
76. Ebara H, Ikezoe J, Johkoh T, et al. Chronic eosinophilic pneumonia: evolution of chest radiograms and CT features. *J Comput Assist Tomogr* **1994**;18:737–744
77. Yoshida K, Shijubo N, Koba H, et al. Chronic eosinophilic pneumonia progressing to lung fibrosis. *Eur Respir J* **1994**;7:1541–1544
78. Storto ML, Kee ST, Golden JA, Webb WR. Hydrostatic pulmonary edema: high-resolution CT findings. *AJR* **1995**;165:817–820
79. Lee JS, Im JG, Ahn JM, Kim YM, Han MC. Fibrosing alveolitis: prognostic implication of ground-glass attenuation at high-resolution CT. *Radiology* **1992**;184:451–454
80. Remy-Jardin M, Giraud F, Remy J, Copin MC, Gosselin B, Duhamel A. Importance of ground-glass attenuation in chronic diffuse infiltrative lung disease: pathologic-CT correlation. *Radiology* **1993**;189:693–698
81. Wells AU, Rubens MB, du Bois RM, Hansell DM. Serial CT in fibrosing alveolitis: prognostic significance of the initial pattern. *AJR* **1993**;161:1159–1165
82. Hartman TE, Primack SL, Kang EU, et al. Disease progression in usual interstitial pneumonia compared with desquamative interstitial pneumonia: assessment with serial CT. *Chest* **1996**;110:378–382
83. Nishimura K, Itoh H, Kitaichi M, Nagai S, Izumi T. Pulmonary sarcoidosis: correlation of CT and histopathologic findings. *Radiology* **1993**;189:105–109
84. Remy-Jardin M, Giraud F, Remy J, Wattinne L, Wallaert B, Duhamel A. Pulmonary sarcoidosis: role of CT in the evaluation of disease activity and functional impairment and in prognosis assessment. *Radiology* **1994**;191:675–680
85. Padley SPG, Adler BD, Staples CA, Miller RR, Müller NL. Pulmonary talcosis: CT findings in three cases. *Radiology* **1993**;186:125–127